FULL PAPER

Magnetic Resonance in Medicine 00:000–000 (2013)

Combined Saturation/Inversion Recovery Sequences for Improved Evaluation of Scar and Diffuse Fibrosis in Patients with Arrhythmia or Heart Rate Variability

Sebastian Weingärtner,[1,2] Mehmet Akçakaya,[1] Tamer Basha,[1] Kraig V. Kissinger,[1] Beth Goddu,[1] Sophie Berg,[1] Warren J. Manning,[1,3] and Reza Nezafat[1]*

Purpose: To develop arrhythmia-insensitive inversion recovery sequences for improved visualization of myocardial scar and quantification of diffuse fibrosis.

Methods: A novel preparation pre-pulse, called saturation pulse prepared heart-rate-independent inversion recovery, is introduced, which consists of a combination of saturation and inversion pulses to remove the magnetization history in each heartbeat in late gadolinium enhancement (LGE) imaging and eliminate the need for rest periods in T_1 mapping. The proposed LGE and T_1 mapping sequences were evaluated against conventional LGE and modified Look-Locker inversion sequences using numerical simulations, phantom and imaging in healthy subjects and patients with suspected or known cardiovascular disease.

Results: Simulations and phantom experiments show that the saturation pulse prepared heart-rate-independent inversion recovery pre-pulse in LGE reduces ghosting artifacts and results in perfect nulling of the healthy myocardium in the presence of arrhythmia. In T_1 mapping, saturation pulse prepared heart-rate-independent inversion recovery results in (a) reduced scan time (17 vs. 9 heartbeats), (b) insensitivity to heart rate for long T_1, and (c) increased signal homogeneity for short T_1. LGE images in a patient in atrial fibrillation during the scan show improved myocardial nulling. In vivo T_1 maps demonstrate increased signal homogeneity in blood pools and myocardium.

Conclusion: The proposed sequences are insensitive to heart rate variability, yield improved LGE images in the presence of arrhythmias, as well as T_1 mapping with shorter scan times. **Magn Reson Med 000:000–000, 2013.** **© 2013 Wiley Periodicals, Inc.**

Key words: scar imaging; atrial fibrillation; T_1 mapping; late gadolinium enhancement; heart rate variability; diffuse fibrosis

Atrial fibrillation (AF) is the most common sustained cardiac arrhythmia and a common co-morbidity in patients with heart failure (1–3). Electrocardiographic (ECG) gated late gadolinium enhancement (LGE) is the current gold standard for evaluation of scar and fibrosis in the left ventricle (LV) (4–6) and the left atrium (7–9) and is commonly performed in these patients. In addition to LGE, myocardial T_1 mapping has recently emerged as a method for imaging of diffuse fibrosis (10,11). However, in the presence of arrhythmias and heart rate variability, LGE and T_1 mapping image quality is usually sub-optimal. Therefore, an approach that takes heart rate variability during the scan into account is desirable for these patient cohorts.

The short time interval between two subsequent inversion pulses in the ECG-triggered LGE sequence does not allow full recovery of the signal and it is directly influenced by variations in the heart rate (12). Hence, the LGE signal is dependent on the length of the previous R-R interval. This signal variation causes a time-varying weighting of k-space data which results in ghosting artifacts (13). Furthermore, the presence of signal variations suggests that the use of a fixed inversion time, pre-selected by a Look-Locker scout (14), is not ideal and may result in incomplete nulling of the healthy myocardium.

For myocardial T_1 mapping, a modified Look-Locker inversion recovery (MOLLI) (15) sequence is the most common approach (16–18). By performing three-to-five data readouts after each preparation pulse, MOLLI incorporates the efficient sampling of the T_1 relaxation curve that was originally proposed by Look and Locker (14). To provide a sufficient number of sampling points to define the T_1 relaxation, three groups of images are acquired, each following a single inversion pulse. The three groups contain 3, 3, and 5 ECG-triggered images, respectively, which are acquired in consecutive heartbeats. Two rest periods of three heart cycles each separate these three groups in order to allow for sufficient recovery of the longitudinal magnetization. These rest cycles decrease the imaging efficiency and require relatively long breath holds (17 heartbeats). Furthermore, the T_1 recovery curve is sampled at time points separated by the R-R interval lengths. This imposes a fixed timing scheme, which results in poor fit conditions for short T_1 times. Moreover, the signal disturbance of the relaxation curve induced by the radiofrequency imaging pulses varies based on the heart rate. For long T_1 times, this results in a pronounced heart rate dependence of the

[1]Department of Medicine, Beth Israel Deaconess Medical Center and Harvard Medical School, Boston, Massachusetts, USA.

[2]Computer Assisted Clinical Medicine, University Medical Center Mannheim, Heidelberg University, Mannheim, Germany.

[3]Department of Radiology, Beth Israel Deaconess Medical Center and Harvard Medical School, Boston, Massachusetts, USA.

Grant sponsor: NIH; Grant number: R01EB008743-01A2; Grant sponsor: Deutsche Telekom Stiftung.

*Correspondence to: Reza Nezafat, Ph.D., Beth Israel Deaconess Medical Center, 330 Brookline Ave, Boston, MA 02215. E-mail: rnezafat@bidmc.harvard.edu

Received 11 October 2012; revised 1 March 2013; accepted 19 March 2013

DOI 10.1002/mrm.24761
Published online in Wiley Online Library (wileyonlinelibrary.com).

estimated T_1 (19). Therefore, improved T_1 mapping sequences with shorter scan time, reduced sensitivity to heart rate and arrhythmia are needed.

Saturation recovery based myocardial T_1 mapping was proposed as a method to avoid signal recovery periods (20–23). A modified Look-Locker sequence using saturation recovery instead of inversion recovery in MOLLI was proposed in (23). Preliminary results with a saturation recovery T_1 mapping method during breath holds, called saturation-recovery single-shot acquisition were demonstrated in (20,21). With saturation-recovery single-shot acquisition, a saturation pulse is applied in every heart beat and the saturation times are varied within the applicable range. This approach is less prone to T_2 induced variations of the T_1 estimation. Recently, a T_1 mapping method was reported using only two single-shot images, one without magnetization preparation and one following saturation recovery (22). The proposed method was found to be less susceptible to heart-rate variations and T_2 changes compared to MOLLI. However, the use of only a saturation pulse reduced the dynamic range, thereby decreasing the fit-conditioning of the T_1 estimation (24,25). This adversely impacts the T_1 map quality and mitigates the advantage drawn from the improved imaging efficiency.

In this study, we sought to develop an improved imaging sequence for assessment of focal fibrosis/scar and diffuse fibrosis in the presence of arrhythmia or heart rate variability. Numerical simulations, phantom experiments, and in vivo imaging in healthy subjects and patients with known or suspected cardiovascular disease, including arrhythmias, are used to evaluate the proposed sequences.

METHODS

Sequence

Figure 1a shows the schematic of the proposed magnetization preparation. A nonselective saturation pulse is applied immediately after the ECG R-wave, nulling the entire magnetization in the volume and erasing the dependence of the longitudinal magnetization on the signal recovery during the preceding R-R intervals. The conventional nonselective inversion pulse is applied after the saturation pulse at time $T_{\mathrm{sat}} - T_{\mathrm{inv}}$, where T_{inv} is the time between the inversion pulse and data sampling, and T_{sat} is the time between the saturation pulse and data sampling. We refer to this magnetization preparation as saturation pulse prepared heart-rate-independent inversion recovery (SAPPHIRE) pre-pulse.

All studies were performed on a 1.5 T Philips Achieva (Philips, Best, The Netherlands) system using either a body coil (for phantom) or a 32-channel cardiac receiver coil for in vivo measurements. In vivo studies were approved by our institutional review board and all subjects provided written informed consent before study participation.

LGE Sequence

In conventional LGE imaging, the signal at time t after an inversion pulse can be described with the Bloch equations as

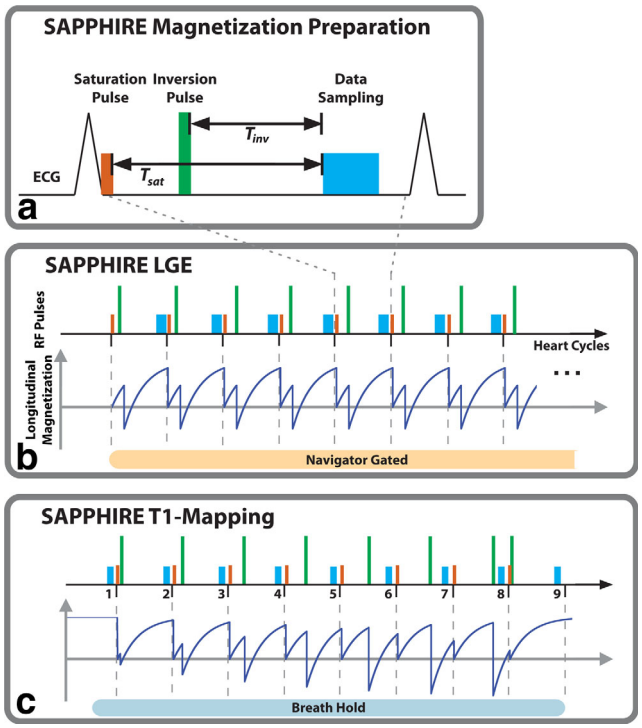

FIG. 1. Sequence diagrams of the proposed sequences: **a:** SAPPHIRE magnetization preparation scheme. A nonselective saturation pulse is applied immediately after the R-wave on the electrocardiogram (ECG). It is followed by a conventional nonselective inversion pulse after time $T_{\mathrm{sat}} - T_{\mathrm{inv}}$ and by the imaging pulses after time T_{sat}. **b**: SAPPHIRE late gadolinium enhancement (LGE) sequence. A navigator-gated segmented 3D LGE sequence was performed, where a SAPPHIRE pre-pulse is applied at every heartbeat, with the constant T_{sat} and T_{inv} times, adjusted to null the healthy myocardial tissue. **c**: SAPPHIRE T_1 mapping. Multiple 2D single-shot images acquired with varying T_{inv} to create various T_1-weighted images are used for calculation of T_1 times by performing a voxel-wise curve fitting to the signal intensity. Characteristic signal curves of the longitudinal magnetization during the application of the pulse sequences are illustrated under the pulse-diagrams.

$$S_{\mathrm{LGE}}(t) = M_0 \left(1 - (1 + M_{\mathrm{h}}) e^{-t/T_1}\right), \qquad [1]$$

where M_0 is the spin-density, T_1 the longitudinal relaxation time of the observed tissue, and M_{h} is the magnetization immediately before the inversion and contains the information about the magnetization history. Full recovery of magnetization in the last heartbeat corresponds to $M_{\mathrm{h}} = 1$. In this case, a tissue with the longitudinal relaxation time T_1 would be nulled $T' = T_1 \cdot \log(2)$ after the inversion time.

Figure 1b shows the sequence diagram of a SAPPHIRE LGE sequence. Here, the signal at the time t after the inversion pulse of a SAPPHIRE LGE sequence can be derived from the Bloch-equations as

$$S_{\mathrm{SAPPHIRE}}(t) = M_0 \left(1 - \left(2 - e^{-(T_{\mathrm{sat}} - T_{\mathrm{inv}})/T_1}\right) e^{-t/T_1}\right), \qquad [2]$$

where M_0 is the spin density, T_1 the longitudinal relaxation time of the observed tissue, and T_{sat} and T_{inv} are as

defined above. If a tissue is nulled in a conventional inversion recovery sequence with full relaxation using the inversion time T', then enforcing $S_{\mathrm{SAPPHIRE}}(T_{\mathrm{inv}}) = 0$ for $T_1 = T'/\log(2)$ would ensure that the same tissue will be nulled using SAPPHIRE LGE. The T_{inv} time of the SAPPHIRE LGE sequence can be derived from this equation, as

$$T_{\mathrm{inv}}(T') = T_{\mathrm{sat}} + T' \left(1 - \frac{\log\left(e^{\log(2)T_{\mathrm{sat}}/T'} + 1\right)}{\log(2)}\right). \quad [3]$$

Equation [3] along with the fact that the sum of T_{sat} and the duration of the saturation pulse equals the cardiac trigger time allows for the unique determination of T_{sat} and T_{inv} for any given T'. The inversion time conversion from Eq. [3] was integrated in the clinical scanner software such that the inversion time required for the SAPPHIRE LGE sequence was automatically calculated from the user-specified inversion time that would be typically used for a conventional LGE sequence.

The nonselective saturation at the beginning of each heart cycle in SAPPHIRE LGE suggests a decreased signal-to-noise ratio (SNR) in the LGE images. Therefore, the application of SAPPHIRE LGE offers the possibility to trade-off an anticipated loss in the SNR of the LGE images for improved robustness to arrhythmia.

T_1 Mapping Sequence

Figure 1c shows the proposed SAPPHIRE T_1 mapping sequence, which consists of nine single-shot images with a SAPPHIRE pre-pulse acquired over nine heart beats. T_{inv} is varied to create images with different T_1-weighted contrasts. A saturation pulse is used immediately after the R wave to remove the dependency on the magnetization history and eliminate the necessity for rest-periods. This reduces the scan time by enabling acquisition in all subsequent heart beats, and allows flexibility in choosing T_{inv} in order to densely sample the early part of the T_1 relaxation curve. The first heart cycle was performed without any magnetization preparation, under the assumption that this corresponds to a fully recovered longitudinal magnetization, and thus to the sampling of the late part of the T_1 curve. The effective inversion times were linearly distributed over the applicable range based on the anticipated T_1 time. To enable the application of longer T_{inv}, the pulse sequence also allows for SAPPHIRE preparation in one heart cycle, and imaging in the subsequent one. After data acquisition, the two-parameter model from Eq. [2] was fitted voxel-wise to the signal intensity to generate the T_1 maps.

Numerical Simulations

In AF, the heart rate varies up to 70% (26), resulting in changes in the R-R interval length. For simulations and phantom measurements, such arrhythmic ECGs were modeled with random R-R interval lengths from a normal distribution with a mean length chosen according to anticipated heart rates (667 ms for 90 beats per minute (bpm)). The standard deviation of the arrhythmias was chosen between 30% and 70% of the mean R-R interval length.

Magnetization Signal Through the LGE Sequence

A numerical simulation was performed to study the behavior of the magnetization signal for the SAPPHIRE LGE sequence in the presence of arrhythmia. The longitudinal relaxation with two different T_1 times was simulated during an ECG in sinus rhythm and an arrhythmic ECG that was implemented as described above, with a heart rate of 90 bpm and a standard deviation of 70% of the mean R-R interval length. The signal was simulated for a conventional LGE sequence and for SAPPHIRE LGE by iteratively applying Eqs. [1] and [2], respectively. The T_1 times chosen for this simulation were 560 ms and 360 ms, which are typical relaxation times at 1.5 T for healthy myocardium and scar tissue, respectively (27). The timing of inversion pulses in the simulated sequences was adjusted in order to null the component with 560 ms T_1 during sinus rhythm. The signal recovery was studied in terms of the relaxation curves of both components, and in terms of the signal level of the component with T_1 of 560 ms at mid-diastole imaging time.

Image Artifacts in LGE Imaging

To study LGE imaging artifacts associated with arrhythmia, a numerical phantom was designed to represent a short-axis LV, and consists of multiple compartments: LV, right ventricle (RV), healthy myocardium, scar, abdomen, cerebrospinal fluid, and fat (cardiac and back). The tissues were represented by T_1 times of 450 ms, 450 ms, 560 ms, 360 ms, 320 ms, 4000 ms, and 70 ms, respectively (27,28). The phantom size was set to $512 \times 512 \times 20$ voxels. Based on Eqs. [1] and [2], we simulated an image acquisition using both conventional LGE and SAPPHIRE LGE sequences. The excitation flip-angle was chosen to be 15°. Ten k-space lines with a repetition time (TR) of 3.6 ms were acquired per heartbeat with a low-to-high k-space ordering in each shot. The trigger delay was chosen to be mid-diastole. The image acquisition was simulated five times with different ECGs. The first simulated ECG was computed with a heart rate of 90 bpm and sinus rhythm. The other experiments were performed with arrhythmic ECGs, where the standard deviation of the random variations were 30%, 40%, 50%, or 60% of the mean R-R interval length, respectively.

Phantom Imaging

Contrast-to-Noise Ratio in LGE

The contrast properties of the SAPPHIRE LGE sequence were quantified on phantom images, and compared with the conventional LGE sequence. The phantom consisted of a bottle filled with water, copper sulfate (0.77 g/L), and sodium chloride (2 g/L) and a number of vials containing different liquids. Three compartments with T_1 times of 560 ms, 450 ms, and 370 ms were selected for analysis. A 2D inversion recovery gradient recalled echo (GRE) sequence (field of view (FOV) = 320×400 mm^2, in-plane resolution = 1.6×1.6 mm^2, slice-thickness = 12 mm, TR/echo time (TE) = 5.1 ms/2.4 ms, flip angle =

25°, acquisition window = 76 ms, segmentation factor = 15, number of averages = 20) was used for conventional LGE imaging. The same sequence equipped with the additional saturation pulse was used as the 2D SAPPHIRE LGE sequence. Imaging was performed with mid-diastole triggering and the sequence timing of both sequences was chosen to null the vial with T_1 of 560 ms. Measurements were performed using seven different simulated ECGs in sinus rhythm with heart rates ranging from 60 to 120 bpm. The inversion time for the conventional LGE sequence was adjusted individually for different heart rates to ensure proper nulling. For each scan, the images were averaged before further processing. The contrast-to-noise ratio (CNR), defined as the difference of the average signal in two regions of interest over the standard deviation of the noise, was assessed between vials with different T_1 times (560 vs. 370 ms, 450 vs. 370 ms). To obtain the standard deviation of the noise, a separate noise measurement was acquired after each imaging sequence. The noise measurement was performed with the same sequence parameters as above, except all gradients and radiofrequency pulses were disabled and only one average was acquired (29).

Image Artifacts in LGE Imaging

To study the LGE imaging artifacts induced by arrhythmias and heart rate variability, the bottle and vial-phantom described above was scanned with a simulated, arrhythmic ECG signal. A 3D inversion recovery GRE sequence with the following parameters was used: FOV = 320 × 400 × 102 mm^3, spatial resolution = 2 × 2 × 6 mm^3, TR/TE = 4.8 ms/2.3 ms, flip angle = 25°, acquisition window = 50 ms, segmentation factor = 10. The time between the inversion pulse and the imaging in the conventional LGE sequence was adjusted to ensure nulling of the phantom compartment with a T_1 time of 560 ms during sinus-rhythm. The timing of the SAPPHIRE LGE sequence was adjusted accordingly using Eq. [3]. Four arrhythmic ECGs with a mean heart rate of 90 bpm and random variations with standard deviations of 30%, 40%, 50%, and 60% of the R-R interval length were simulated.

T_1 Mapping During Heart Rate Variations

A phantom consisting of multiple vials containing Mn-doped water of different concentrations (30) was scanned using the SAPPHIRE T_1 and MOLLI T_1 mapping sequences. Multiple ECGs were simulated in sinus-rhythm with heart rates ranging from 50 bpm to 110 bpm. An SSFP sequence with the following parameters was used: 2D single-slice, FOV = 300 × 300 mm^2, in-plane resolution = 1.7 × 2.1 mm^2, slice-thickness = 10 mm, TR/TE = 2.6 ms/1.0 ms, flip angle = 35°, acquisition window = 190 ms, segmentation factor = 73, linear k-space ordering. A spin-echo inversion recovery sequence with the same geometrical parameters with TR/TE = 15 s/10 ms was acquired as a reference. SAPPHIRE T_1 mapping and MOLLI were evaluated in terms of accuracy with respect to the spin echo reference, using the unpaired *t*-test. A *P* value less than 0.05 was considered to be significant. The correlation between the estimated T_1 times and the heart rate was studied using Pearson's linear correlation coefficient.

Analysis of the Homogeneity of the T_1 Estimates

Due to the altered SNR in the T_1-weighted images and the differences in the sampling of the longitudinal magnetization recovery curve, the noise-performance of SAPPHIRE T_1 mapping is not necessarily analogous to conventional MOLLI T_1. Thus, phantom measurements were performed to study the T_1 homogeneity of SAPPHIRE T_1 maps and MOLLI T_1 maps. The effects were measured at different noise levels by using a 2D single-slice acquisition with one to three averages: FOV = 300 × 300 mm^2, in-plane resolution = 1.7 × 2.1 mm^2, slice-thickness = 3 mm, TR/TE = 2.6 ms/1.0 ms, flip angle = 35°, acquisition window = 190 ms, segmentation factor = 73, linear k-space ordering. The standard deviation of T_1 measurements within each phantom compartment was used to assess the homogeneity as a surrogate for noise-resilience, because the T_1 times can be assumed to be homogenous.

In Vivo Imaging

LGE Imaging in Patients with Arrhythmia

To demonstrate the feasibility of SAPPHIRE LGE, 5 patients (3 males, 58 ± 23 years) with history of AF were recruited. Among these patients, only one with chronic AF (male, 53 years) was in AF during the examination, while the rest were in sinus rhythm. Both conventional LGE and SAPPHIRE LGE were acquired in a random order, in all subjects. For the patient in AF during the scan, the image acquisitions for conventional LGE and SAPPHIRE LGE were repeated in 20 min with reversed order.

LGE imaging was performed on the short-axis of the heart, after the administration of 0.2 mmol/kg gadopentetate dimeglumine (Magnevist, Bayer Schering Pharma AG, Berlin, Germany). The sequences shared the following parameters: FOV = 320 × 400 × 100 mm^3, in-plane resolution = 1.5 × 1.5 × 4 mm^3, TR/TE = 5.1 ms/2.5 ms, flip angle = 25°, acquisition window = 129 ms, segmentation factor = 25. To provide proper nulling, the inversion time was extracted from a Look-Locker scout for the conventional sequence and from a single-slice T_1 map acquired with MOLLI for SAPPHIRE LGE. Furthermore, the ECG of the subject with chronic AF was analyzed in terms of average, maximum and minimum heart rate and heart rate variability.

T_1 Mapping

Eleven healthy adult subjects (5 males; 31 ± 14 years) and nine patients with suspected or known cardiac diseases (5 males; 55 ± 19 years) were recruited. All healthy subjects were imaged 5–15 min after administration of 0.2 mmol/kg of gadobenate dimeglumine (MultiHance; Bracco, Milan, Italy). For the patient examinations, the T_1 mapping sequence was integrated in the clinical scan protocol, following the injection of 0.1 mmol/kg of the gadobenate dimeglumine (our standard clinical contrast dose). Images were acquired on the

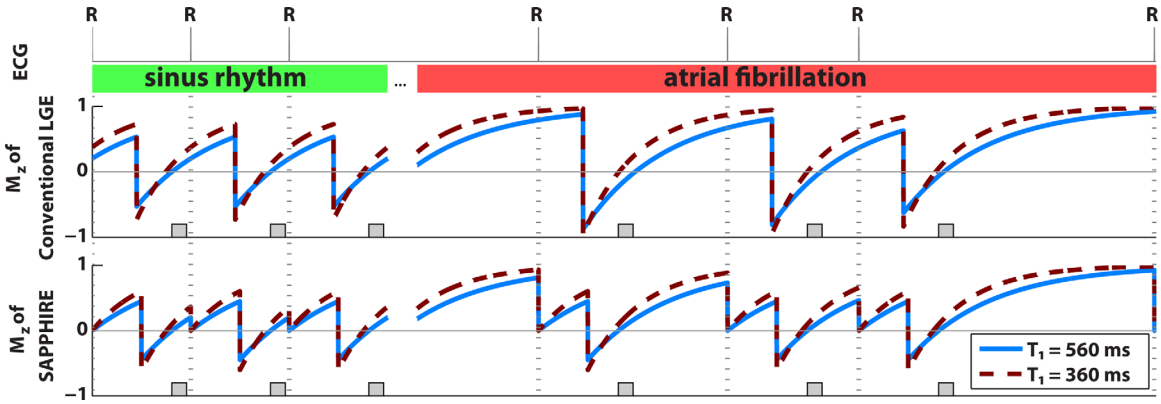

FIG. 2. Numerical simulations demonstrating the disturbance in the signal recovery curves of different tissues induced by an arrhythmia such as atrial fibrillation (AF). An ECG with a heart rate of 90 bpm in sinus rhythm and normally distributed variations with a standard deviation of 70% of the mean R-R interval length in nonsinus rhythm was simulated for atrial fibrillation. The gray blocks indicate the time and duration of mid-diastole imaging. For both sequences, the signal always relaxes to the same level during sinus-rhythm (left panel). However, with AF, the signal before the inversion time and at the imaging time varies substantially for the conventional LGE, while it remains constant for SAPPHIRE LGE.

short-axis of the heart. SAPPHIRE T_1 mapping was used with nine images per slice and was compared with the optimized MOLLI T_1 scheme proposed in (31). The sequence parameters were: FOV = 300 × 300 mm^2, in-plane resolution = 1.7 × 2.1 mm^2, slice-thickness = 10 mm, number of short-axis slices = 3, TR/TE = 2.6 ms/1.0 ms, flip angle = 35°, acquisition window = 190 ms, segmentation factor = 73, linear k-space ordering. The breath hold duration ranged from 7 s to 10 s for SAPPHIRE T_1 mapping and 13 s to 19 s for MOLLI.

A quantitative analysis of the estimated T_1 times was performed separately for the subgroup of healthy subjects and patients. Regions of interest were manually drawn for the myocardium, LV and RV blood pools. For each subgroup, the average T_1 times were calculated. The homogeneity of T_1 maps was assessed by calculating the standard deviation of the T_1 signal in the blood pools. The measurements from MOLLI T_1 and SAPPHIRE T_1 were compared using a paired *t*-test. A *P* value of less than 0.05 was considered significant.

RESULTS

Numerical Simulations

Magnetization Signal Through the LGE Sequence

The longitudinal magnetization (M_z) during sinus rhythm and AF is depicted in Figure 2. During sinus rhythm, the magnetization relaxes to the same signal level in each heartbeat for both conventional LGE and SAPPHIRE LGE. However, in the presence of arrhythmia the signal level right before the inversion pulse shows major variances for conventional LGE. The SAPPHIRE LGE signal right before the inversion pulse does not vary, because the magnetization history is reset by the saturation pulse.

Figure 3 shows the actual signal of the intended nulled component (T_1 = 560 ms). This simulation indicates that despite the varying extent of the signal relaxation, the SAPPHIRE LGE sequence ensures a reliable nulling of the component. However, during arrhythmia, the actual signal in conventional LGE deviates by up to 40% of the spin-density with respect to proper nulling.

Image Artifacts in LGE Imaging

Figure 4 shows the results of the simulations with the numerical phantom. The first column (Fig. 4a,f) shows the artifact free images, acquired during sinus rhythm, using conventional LGE and SAPPHIRE LGE, respectively. The first row shows the conventional LGE images (Fig. 4a–e), where significant ghosting artifacts are readily visible even for 30% arrhythmia. The artifacts become more significant as the standard deviation of the random variations in the R-R interval length increases. The tissues with long T_1 times (myocardium and CSF) result in more pronounced ghosting than tissues with very short T_1 times such as fat. In addition to the ghosting artifacts, significant signal changes and incomplete nulling is observed. However, the SAPPHIRE LGE images (Fig. 4f–j) are free from ghosting artifacts and provide complete myocardial nulling for all simulated ECGs.

Phantom Imaging

Contrast-to-Noise Ratio in LGE

Table 1 summarizes the quantitative results of the CNR measurements. In phantom studies, SAPPHIRE CNR was reduced by 22–39% compared with conventional LGE. The contrast loss between both sets of vials (T_1 times 560 vs. 370 ms, and 450 vs. 370 ms) show the same trend and are in the same range. The minimum loss in CNR is observed with a heart rate of 80 bpm (23%, for 560 vs. 370 ms) and increases for higher heart rates up to (39%, for 560 vs. 370 ms) at 120 bpm.

Image Artifacts in LGE Imaging

Figure 5 shows the images of the phantom with and without simulated arrhythmias using both conventional LGE and SAPPHIRE LGE. The upper right vial (T_1 = 560 ms)

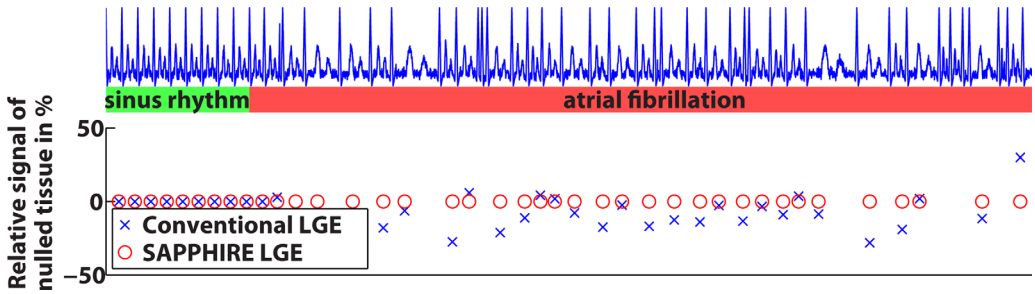

FIG. 3. Signal changes induced by arrhythmia in conventional LGE and SAPPHIRE LGE. An ECG with a mean heart rate of 90 bpm was simulated and random variations in the R-R interval length were added during AF (upper part). The inversion time was chosen to null the signal in sinus rhythm (T_1 = 560 ms). The lower part shows the signal relative to the spin-density is correctly nulled during sinus rhythm. However, deviations by up to 40% can be observed for the conventional LGE during AF. SAPPHIRE LGE successfully nulls the signal independent of the rhythm.

was attempted to be nulled with both sequences. As with the numerical simulations, the ghosting artifacts were present for all arrhythmia levels with the conventional LGE sequence (Fig. 5b–e). Furthermore, the signal level in the upper right vial is substantially increased and other phantom compartments are randomly nulled in the presence of arrhythmia. In contrast, SAPPHIRE LGE images (Fig. 5g–j) show no visible ghosting artifacts and complete nulling of the upper right vial regardless of the arrhythmia level, providing an acquisition robust to heart rate variations.

T_1 Mapping During Heart Rate Variations

Figure 6 shows the T_1 times determined in several vials with SAPPHIRE T_1 and MOLLI T_1 as a function of the heart rate. For short T_1 times in the post-contrast range, SAPPHIRE T_1 and MOLLI T_1 show small relative deviations of 0.2–4.4% ($P > 0.16$) and 1.0–3.9% ($P < 0.001$) from the spin echo sequence, respectively. For longer T_1 times, the relative difference between SAPPHIRE T_1 and the reference is 1.1–4.4%, where SAPPHIRE T_1 times are significantly longer ($P < 0.001$), whereas MOLLI T_1 significantly underestimated T_1 with respect to the spin-echo sequence ($P < 0.01$). The underestimation with MOLLI T_1 worsens at higher heart rates and leads to a relative error of up to 19%. MOLLI T_1 times above 600 ms show major correlation to the heart rate ($R^2 > 0.98$), whereas no significant correlation was found for SAPPHIRE T_1 ($R^2 < 0.49$).

Analysis of the Homogeneity of the T_1 Estimates

Figure 7 shows the results of the homogeneity of the T_1 maps in phantom measurements. The variation decreases with an increased number of averages (increased underlying SNR), indicating that signal homogeneity provides a representation of the noise-performance. SAPPHIRE T_1 reduces the standard deviation of the T_1 times by 25–37% for different number of averages and a short T_1 time of 220 ms compared with MOLLI T_1. For longer T_1 times, the differences between the two sequences in terms of the variability of T_1 times are reduced (7–29% at 350 ms, −16% to 9% at 450 ms for number of averages varying between 3 and 1).

In Vivo Imaging

LGE Imaging in Patients with Arrhythmia

Figure 8a shows representative slices of the SAPPHIRE LGE acquired in a patient with chronic AF. Imaging with

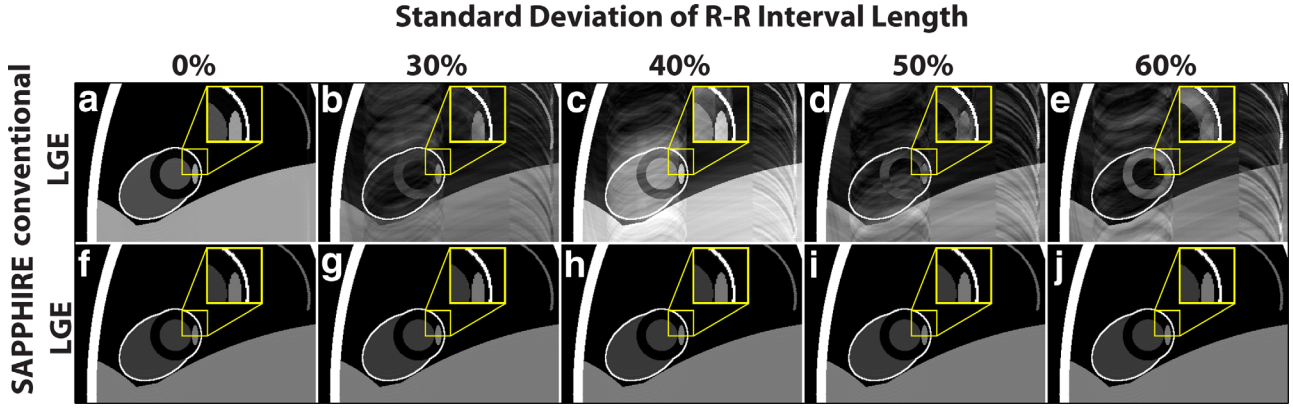

FIG. 4. Numerical simulations to study arrhythmia induced imaging artifacts for the conventional LGE (**a–e**) and SAPPHIRE LGE (**f–j**). An ECG signal with the average heart rate of 90 bpm was randomly disturbed by arrhythmias of normally distributed values whose standard deviation varied between 30% and 60% of the average R-R interval length. The conventional LGE images are contaminated with ghosting artifacts and show substantial contrast alterations and imperfect nulling for all levels of arrhythmias. The SAPPHIRE LGE images remain free from ghosting artifacts and provide complete nulling of the healthy myocardium.

Table 1
Loss in Contrast-to-Noise Ratio (CNR) Between Different Vials (T_1 of 560 vs. 370 ms, 450 vs. 370 ms) by Using SAPPHIRE LGE Compared with Conventional LGE (i.e., ($CNR_{SAPPHIRE} - CNR_{LGE}$)/$CNR_{LGE}$) at Different Heart Rates in Phantom

Heart rate (bpm)	%CNR loss 560 vs. 370	%CNR loss 450 vs. 370
60	23.0	21.5
70	25.5	24.5
80	22.9	22.6
90	27.0	27.7
100	30.4	29.7
110	34.9	34.0
120	38.8	38.4

The sequence timing was adjusted to null the vial with 560 ms T_1 and imaging was performed at mid-diastole triggering of simulated electrocardiogram (ECG).

conventional LGE and SAPPHIRE LGE was performed 27 and 19 min after contrast injection, respectively. The subject's mean heart rate during the scan was 76 bpm. The heart rate varied between 34 and 104 bpm, with a standard deviation of 12 bpm and an interquartile range of 16 bpm. An excerpt of the patient's ECG is shown in Figure 8b,c. Anterolateral and inferolateral subendocardial based LGE was observed with both sequences. Ghosting artifacts can be seen in the blood pools with conventional LGE. Furthermore, the conventional LGE images had incomplete nulling of the septal myocardium (Fig. 8a). The SAPPHIRE LGE images were visually free from ghosting artifacts caused by heart rate variations and complete nulling of the healthy myocardium was achieved. The repeated scans, which were performed 36 and 43 min after contrast injection for conventional LGE and SAPPHIRE LGE, respectively, showed the same artifacts and incomplete nulling of healthy myocardium.

T_1 Mapping

Figure 9 shows representative SAPPHIRE T_1 and MOLLI T_1 maps acquired after injection of 0.2 mmol/kg gadobenate dimeglumine in a healthy subject. The SAPPHIRE T_1 blood pools and myocardium have visually improved homogeneity compared with MOLLI T_1. Figure 10 shows T_1 maps from two patients referred to cardiac MR for suspected hypertrophic cardiomyopathy (Patient #1) and with heart failure (Patient #2). Images were acquired 10 and 15 min after contrast injection of 0.1 mmol/kg gadobenate dimeglumine, respectively. In the region of interest-based analysis, the average T_1 in the myocardium and the LV and RV blood pools showed no significant difference between the two sequences, for either of the subgroups ($P > 0.13$, relative mean difference: myocardium $< 3.0\%$, LV $< 0.6\%$, RV $< 10\%$ for the healthy subgroup; $P > 0.70$, relative mean difference: myocardium $< 1.3\%$, LV $< 1.0\%$, RV $< 0.3\%$). However, SAPPHIRE T_1 led to reductions of the blood pool signal variation of 86% for the healthy subjects (i.e., high-dose subgroup) ($P = 0.051$) and of 44% for the patients (i.e., low-dose subgroup) ($P < 0.02$) compared with MOLLI.

DISCUSSION

In this study, we proposed and demonstrated a combination of saturation and inversion pulses as a novel magnetization preparation for superior LGE and T_1 mapping in the presence of arrhythmias and heart rate variability. Simulation results and phantom measurements showed that the SAPPHIRE LGE sequence is not susceptible to varying signal recovery caused by arrhythmia and heart rate changes, and the in vivo data indicated a robust image quality with improved myocardial signal nulling for patients with arrhythmia. The SAPPHIRE T_1 mapping

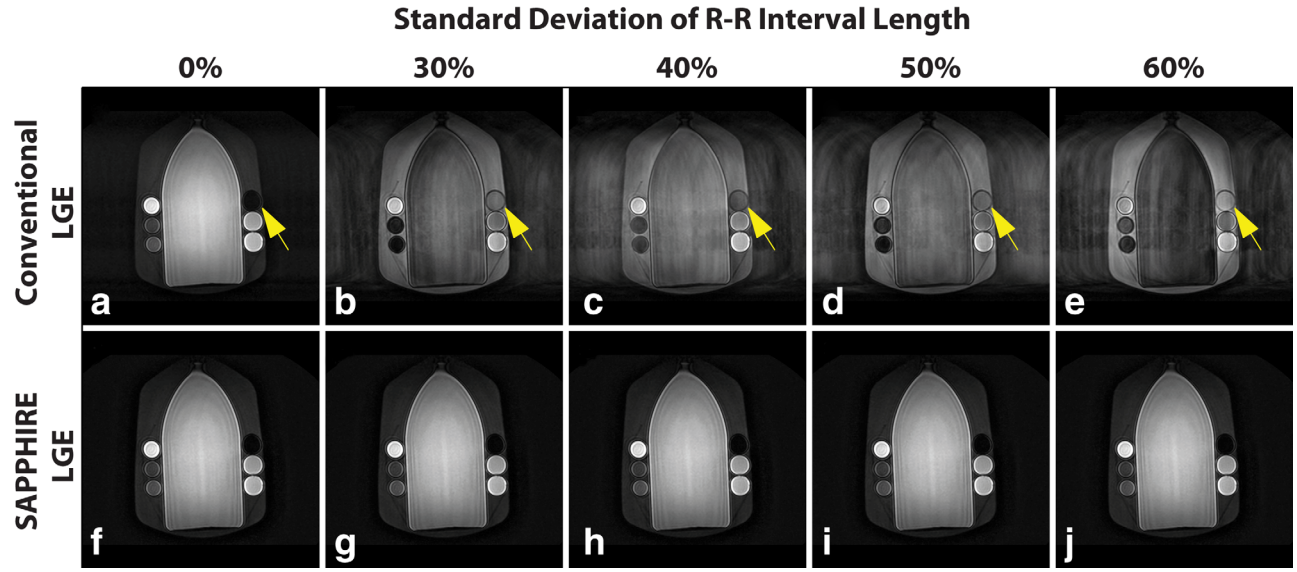

FIG. 5. Phantom measurements to study arrhythmia induced imaging artifacts for conventional LGE (**a–e**) and the SAPPHIRE LGE sequence (**f–j**). Simulated ECGs were generated with the average heart rate of 90 bpm and randomly distributed arrhythmias, whose standard deviation varied between 30 and 60% of the average R-R interval length. For all levels of arrhythmia, ghosting artifacts are readily visible in the conventional LGE images and the signal nulling is substantially compromised (yellow arrows). The SAPPHIRE LGE images are free from any ghosting artifacts, while maintaining the desired contrast and nulling.

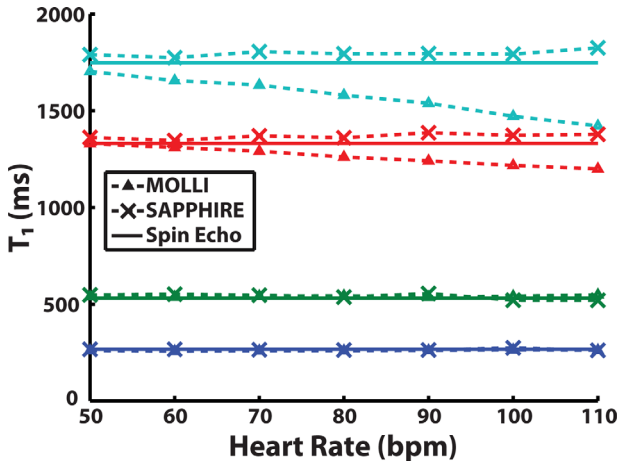

FIG. 6. Phantom T_1 times calculated from MOLLI T_1 and SAPPHIRE T_1, compared to a reference spin-echo inversion recovery sequence at various heart rates and different T_1 times. The MOLLI T_1 times demonstrate an underestimation with significant correlation to the heart rate for long T_1 times ($R^2 > 0.98$). No such underestimation or correlation is seen for SAPPHIRE T_1 ($R^2 < 0.49$).

sequence was shown to provide heart rate invariance, and required shorter breath holds than MOLLI.

Although the ghosting artifacts caused by varying signal recovery are reduced by using SAPPHIRE, residual artifacts can still occur in the presence of arrhythmias, due to cardiac motion. Standard arrhythmia rejection approaches (32) may mitigate this problem, although this was not investigated in our study. The SAPPHIRE LGE sequence can easily be used in combination with clinically available arrhythmia rejection methods to further reduce the impact of these cardiac motion artifacts.

The altered longitudinal relaxation in SAPPHIRE LGE compared with conventional LGE necessitates an explicit computation of T_{inv} in order to null the same tissue. This timing uniquely depends on the tissue T_1 and the cardiac trigger delay. We derived the timing equation for SAPPHIRE LGE from the Bloch-equations that describe the T_1 relaxation. To facilitate the clinical utility of SAPPHIRE LGE, we integrated an automatic inversion time conversion. This allows the operator to specify the inversion time as for a conventional LGE sequence.

As shown in phantom experiments, SAPPHIRE LGE results in a decreased CNR between the tissues of interest compared with conventional LGE. This is because the time for recovery after the initial saturation pulse is shorter than the recovery time between two inversion pulses with conventional LGE. The amount of CNR loss depends on the relation between the heart rate and the trigger delay time. A longer trigger delay allows more recovery after the SAPPHIRE saturation pulse, but does not affect the signal of conventional LGE. Conversely, longer cardiac cycles allow for more signal regrowth after the previous inversion pulse in conventional LGE, but do not affect the SAPPHIRE LGE sequence. Despite the reduced CNR, SAPPHIRE images allowed clear depiction of the fibrosis/scar regions in the chronic AF patient. Further studies with a larger number of patients are needed to investigate if the reduced CNR will have any impact in quantitative or qualitative interpretation of scar.

The phase-sensitive inversion-recovery technique has been proposed to address the imperfect inversion time of conventional LGE (33). Phase-sensitive inversion-recovery recovery relies on the interleaved acquisition of a phase map, which can be used to restore the signal polarity. Although not studied, the proposed SAPPHIRE sequence could potentially be combined with phase-sensitive inversion-recovery by interleaving the acquisition of a phase map with the SAPPHIRE LGE image acquisition. Such approaches should be further studied.

In T_1 mapping, the conditioning of the parameter fit determines the quality of the T_1 map. The fit conditioning depends on the number and distribution of the sampling points across the magnetization recovery curve. With MOLLI T_1, the effective inversion times are determined by the R-R interval length, in such a way that only three images, corresponding to the first image of each imaging group, are acquired with inversion times shorter than the R-R interval length, while the other eight images have longer inversion times. In T_1 mapping following contrast injection, where the T_1 times range from 100 to 600 ms, the longitudinal magnetization is largely recovered for inversion times much longer than the R-R interval length. Hence, these latter eight sample points are largely insensitive to the actual T_1 parameter, and thus do not improve the fit conditioning for the T_1 estimation optimally. With SAPPHIRE T_1 mapping, the saturation pulse removes the recovery periods (thus shortening the scan time) and also enables an arbitrary distribution of the inversion times over the applicable range. Hence, a denser sampling of the beginning of the relaxation curve, which is highly susceptible to the T_1 parameter, is enabled. This results in T_1 maps of high quality, with a prominent improvement over MOLLI T_1

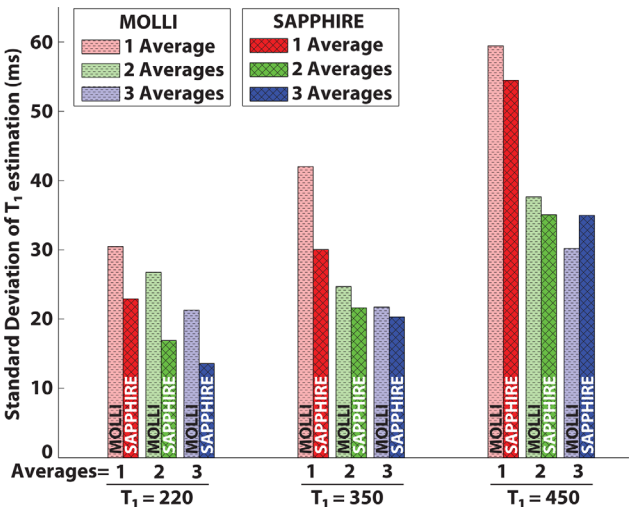

FIG. 7. Homogeneity of T_1 times in different compartments of a phantom, as determined using MOLLI T_1 and SAPPHIRE T_1 mapping based on images with varying SNRs. The homogeneity was measured as the standard deviation of the T_1 times within the phantom compartment. The SNR was varied by using multiple numbers of averages. SAPPHIRE T_1 mapping is shown to increase the homogeneity, especially for short T_1 times.

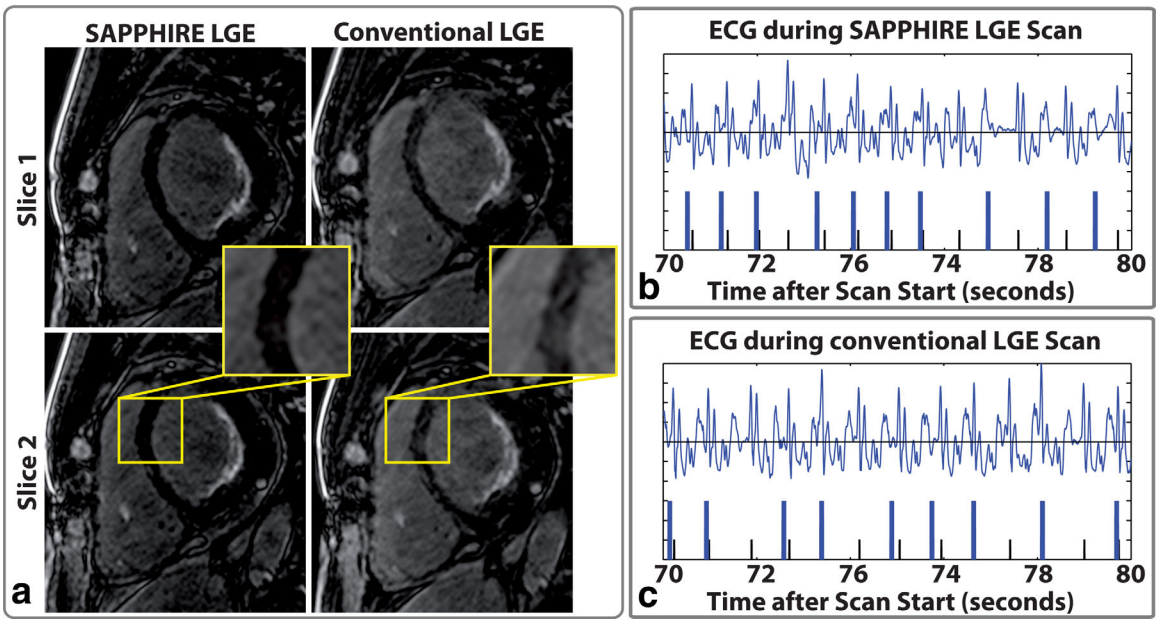

FIG. 8. **a**: Selected slices from a 3D dataset acquired with SAPPHIRE LGE and a conventional LGE in a patient with chronic AF and prior myocardial infarction 10 min after injection of 0.2 mmol/kg gadopentatate dimeglumine. Subendocardial LGE in the anterolateral and inferolateral walls is depicted with both sequences. The magnification shows an area where incomplete signal-nulling occurs in the conventional LGE sequence. The panels (**b**) and (**c**) show the ECG signal recorded during the respective scan. The black ticks indicate the detection of an R-wave and the blue blocks the ECG triggered acquisition windows.

mapping in terms of signal homogeneity and noise resilience, for short post-contrast T_1 times, as obtained after the administration of a high dose of contrast-agent. This advantage reduces for the estimation of longer T_1 times.

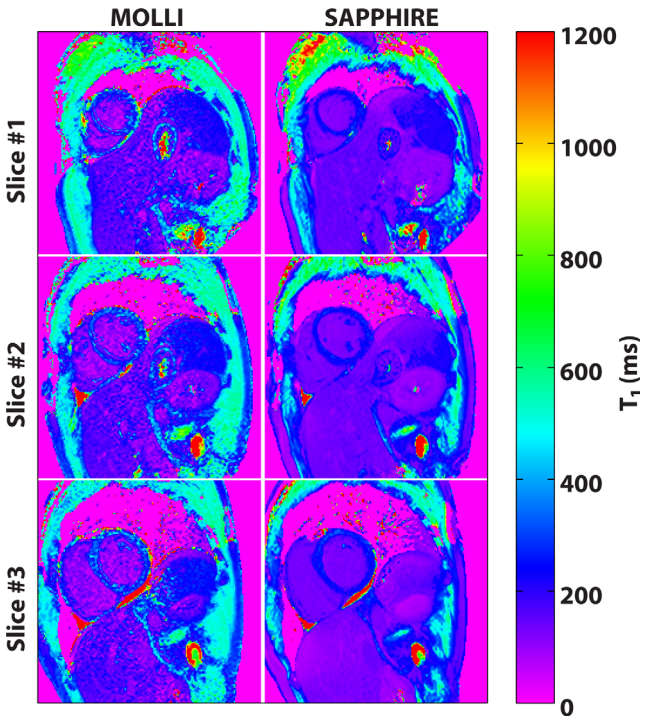

FIG. 9. Multislice 2D T_1 maps acquired in a healthy subject 5 min after administration of 0.2 mmol/kg of gadobenate dimeglumine. Visually higher image quality with more homogenous myocardial and blood signal can be seen in the SAPPHIRE T_1 maps.

In T_1 mapping schemes based on the Look-Locker method, the magnetization relaxation is sampled multiple times after a single preparation. Each set of contiguous imaging excitations induces a signal disturbance, such that a corrupted curve is sampled. Attempts were made to retrospectively correct for these corruptions numerically (34–36). However, in MOLLI, the time points of these corruptions are predetermined by the ECG triggering. Phantom results have shown that this imposes a strong heart-rate dependence on the estimation of long T_1 times with the MOLLI sequence. Recently, it has also been shown that these perturbations

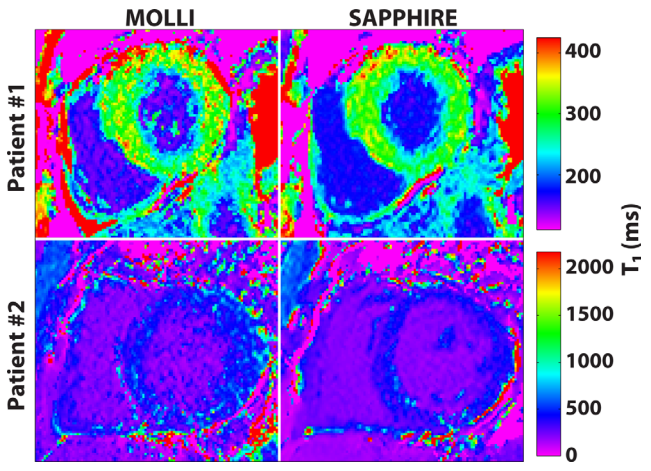

FIG. 10. 2D T_1 maps acquired in two subjects 10 and 15 min (Patient #1 and Patient #2, respectively) after contrast administration of 0.1 mmol/kg of gadobenate dimeglumine using SAPPHIRE T_1 and MOLLI T_1. More homogenous myocardial and blood signal is seen with SAPPHIRE T_1 maps.

are dependent on the spin-spin relaxation time of the tissue, resulting in a T_2 dependence of MOLLI T_1 times (20–22). It has been shown that the sampling of a less corrupted curve, by acquiring only one single-shot image per magnetization preparation, avoids these weaknesses. SAPPHIRE T_1 mapping also allows for only one single-shot image after each magnetization preparation, resulting in no heart-rate dependence of the estimated T_1 times. Similar to other sequences with one single-shot image per magnetization preparation (20–22), no numerically correction for the radiofrequency induced perturbation on the recovery curve was performed.

In addition to heart rate dependency, myocardial T_1 mapping suffers from other challenges. Respiratory and cardiac motion will adversely impact the T_1 fit, resulting in voxels with inaccurate measurements in areas of tissue transition. This will impact the quantitative nature of this imaging sequence where segmental analysis of T_1 is used for evaluation of diffuse fibrosis in each myocardial segment. In addition, slice profile and flip angle may adversely impact the T_1 estimates (37). The use of SSFP imaging for readout also makes this sequence very susceptible to various imaging artifacts, which should be taken into account for accurate T_1 measurements.

Our study has several limitations. We have studied only a very small number of patients, and a larger comparison study is underway. There is no gold standard for evaluation of diffused fibrosis, except invasive biopsies, which has its own limitations. Our study only shows more homogenous T_1 maps with fewer artifacts in the myocardium and the blood pools, and shorter breath hold durations that show no correlation with the heart rate. Further studies correlating the calculated T_1 maps with pathology are required.

CONCLUSIONS

SAPPHIRE preparation reduces the impact of arrhythmia in creating ghosting artifacts and imperfect myocardial signal nulling in LGE and yields more homogenous T_1 maps for short T_1 times in a reduced breath hold duration compared with MOLLI.

ACKNOWLEDGMENTS

S.W. is supported by a fellowship from the Deutsche Telekom Stiftung.

REFERENCES

1. Calkins H, Brugada J, Packer DL, et al. HRS/EHRA/ECAS Expert consensus statement on catheter and surgical ablation of atrial fibrillation: recommendations for personnel, policy, procedures and follow-up: a report of the Heart Rhythm Society (HRS) task force on catheter and surgical ablation of atrial fibrillation. Developed in partnership with the European Heart Rhythm Association (EHRA) and the European Cardiac Arrhythmia Society (ECAS); in collaboration with the American College of Cardiology (ACC), American Heart Association (AHA), and the Society of Thoracic Surgeons (STS). Endorsed and approved by the governing bodies of the American College of Cardiology, the American Heart Association, the European Cardiac Arrhythmia Society, the European Heart Rhythm Association, the Society of Thoracic Surgeons, and the Heart Rhythm Society. Heart Rhythm 2007;4:816–861.
2. Fuster V, Rydén LE, Cannom DS, et al. ACC/AHA/ESC 2006 guidelines for the management of patients with atrial fibrillation. Circulation 2006;114:257–354.
3. Roger VL, Lloyd-Jones DM, Benjamin EJ, et al. Heart disease and stroke statistics—2012 update. Circulation 2012;125:e2–e220.
4. Kim RJ, Fieno DS, Parrish TB, Harris K, Chen E-L, Simonetti O, Bundy J, Finn JP, Klocke FJ, Judd RM. Relationship of MRI delayed contrast enhancement to irreversible injury, infarct age, and contractile function. Circulation 1999;100:1992–2002.
5. Kim RJ, Wu E, Rafael A, Chen EL, Parker MA, Simonetti O, Klocke FJ, Bonow RO, Judd RM. The use of contrast-enhanced magnetic resonance imaging to identify reversible myocardial dysfunction. N Engl J Med 2000;343:1445–1453.
6. Yan AT, Shayne AJ, Brown KA, Gupta SN, Chan CW, Luu TM, Di Carli MF, Reynolds HG, Stevenson WG, Kwong RY. Characterization of the peri-infarct zone by contrast-enhanced cardiac magnetic resonance imaging is a powerful predictor of post–myocardial infarction mortality. Circulation 2006;114:32–39.
7. Peters DC, Wylie JV, Hauser TH, Kissinger KV, Botnar RM, Essebag V, Josephson ME, Manning WJ. Detection of pulmonary vein and left atrial scar after catheter ablation with three-dimensional navigator-gated delayed enhancement MR imaging: initial experience. Radiology 2007;243:690–695.
8. Peters DC, Wylie JV, Hauser TH, et al. Recurrence of atrial fibrillation correlates with the extent of post-procedural late gadolinium enhancement: a pilot study. JACC Cardiovasc Imaging 2009;2:308–316.
9. Oakes RS, Badger TJ, Kholmovski EG, et al. Detection and quantification of left atrial structural remodeling with delayed-enhancement magnetic resonance imaging in patients with atrial fibrillation. Circulation 2009;119:1758–1767.
10. Iles L, Pfluger H, Phrommintikul A, Cherayath J, Aksit P, Gupta SN, Kaye DM, Taylor AJ. Evaluation of diffuse myocardial fibrosis in heart failure with cardiac magnetic resonance contrast-enhanced T_1 mapping. J Am Coll Cardiol 2008;52:1574–1580.
11. Messroghli DR, Nordmeyer S, Dietrich T, Dirsch O, Kaschina E, Savvatis K, Oh-I D, Klein C, Berger F, Kuehne T. Assessment of diffuse myocardial fibrosis in rats using small-animal Look-Locker inversion recovery T_1 mapping. Circ Cardiovasc Imaging 2011;4:636–640.
12. Kim RJ, Shah DJ, Judd RM. How we perform delayed enhancement imaging. J Cardiovasc Magn Reson 2003;5:505–514.
13. Vallée J-P, MacFall JR, Lazeyras F, Wheeler T, Hedlund LW, Spritzer CE, Coleman RE, Sostman HD. Pitfalls in myocardial perfusion assessment with dynamic MR imaging after administration of a contrast material bolus in dogs. Acad Radiol 1999;6:512–520.
14. Look DC, Locker DR. Time saving in measurement of NMR and EPR relaxation times. Rev Sci Instrum 1970;41:250–251.
15. Messroghli DR, Radjenovic A, Kozerke S, Higgins DM, Sivananthan MU, Ridgway JP. Modified Look-Locker inversion recovery (MOLLI) for high-resolution T_1 mapping of the heart. Magn Reson Med 2004;52:141–146.
16. Messroghli DR, Walters K, Plein S, Sparrow P, Friedrich MG, Ridgway JP, Sivananthan MU. Myocardial T_1 mapping: application to patients with acute and chronic myocardial infarction. Magn Reson Med 2007;58:34–40.
17. Nacif MS, Turkbey EB, Gai N, et al. Myocardial T_1 mapping with MRI: comparison of look-locker and MOLLI sequences. J Magn Reson Imaging 2011;34:1367–1373.
18. Schelbert EB, Testa SM, Meier CG, et al. Myocardial extravascular extracellular volume fraction measurement by gadolinium cardiovascular magnetic resonance in humans: slow infusion versus bolus. J Cardiovasc Magn Reson 2011;13:16.
19. Messroghli DR, Plein S, Higgins DM, Walters K, Jones TR, Ridgway JP, Sivananthan MU. Human myocardium: single-breath-hold MR T_1 mapping with high spatial resolution—reproducibility study. Radiology 2006;238:1004–1012.
20. Chow K, Flewitt J, Pagano J, Green J, Friedrich M, Thompson R. MOLLI T_1 values have systematic T_2 and inversion efficiency dependent errors. In Proceedings of the 20th Annual Meeting of ISMRM, Melbourne, Australia, 2012. p. 3288.
21. Chow K, Flewitt J, Pagano J, Green J, Friedrich M, Thompson R. T_2-dependent errors in MOLLI T_1 values: simulations, phantoms, and in vivo studies. J Cardiovasc Magn Reson 2012;14:1–2.
22. Fitts M, Breton E, Kholmovski EG, Dosdall DJ, Vijayakumar S, Hong KP, Ranjan R, Marrouche NF, Axel L, Kim D. Arrhythmia insensitive

rapid cardiac T_1 mapping pulse sequence. Magn Reson Med 2012. doi: 10.1002/mrm.24586.
23. Song T, Stainsby JA, Ho VB, Hood MN, Slavin GS. Flexible cardiac T_1 mapping using a modified Look–Locker acquisition with saturation recovery. Magn Reson Med 2012;67:622–627.
24. Crawley AP, Henkelman RM. A comparison of one-shot and recovery methods in T_1 imaging. Magn Reson Med 1988;7:23–34.
25. Steinhoff S, Zaitsev M, Zilles K, Shah NJ. Fast T_1 mapping with volume coverage. Magn Reson Med 2001;46:131–140.
26. Waktare JEP. Atrial fibrillation. Circulation 2002;106:14–16.
27. Coniglio A, Di Renzi P, Vilches Freixas G, et al. Multiple 3D inversion recovery imaging for volume T_1 mapping of the heart. Magn Reson Med 2012;69:163–170.
28. Hopkins AL, Yeung HN, Bratton CB. Multiple field strength in vivo T_1 and T_2 for cerebrospinal fluid protons. Magn Reson Med 1986;3:303–311.
29. Hu P, Chuang ML, Ngo LH, Stoeck CT, Peters DC, Kissinger KV, Goddu B, Goepfert LA, Manning WJ, Nezafat R. Coronary MR imaging: effect of timing and dose of isosorbide dinitrate administration. Radiology 2010;254:401–409.
30. de Bazelaire CMJ, Duhamel GD, Rofsky NM, Alsop DC. MR imaging relaxation times of abdominal and pelvic tissues measured in vivo at 3.0 T: preliminary results. Radiology 2004;230:652–659.
31. Messroghli DR, Greiser A, Fröhlich M, Dietz R, Schulz-Menger J. Optimization and validation of a fully-integrated pulse sequence for modified Look-Locker inversion recovery (MOLLI) T_1 mapping of the heart. J Magn Reson Imaging 2007;26:1081–1086.
32. Bellenger NG, Pennell DJ. Assessment of cardiac function. Cardiovascular magnetic resonance. Edinburgh, UK: Churchill Livingstone; 2002. pp 99–111.
33. Kellman P, Arai AE, McVeigh ER, Aletras AH. Phase-sensitive inversion recovery for detecting myocardial infarction using gadolinium-delayed hyperenhancement. Magn Reson Med 2002;47:372–383.
34. Cooper MA, Nguyen TD, Spincemaille P, Prince MR, Weinsaft JW, Wang Y. Flip angle profile correction for T_1 and T_2 quantification with look-locker inversion recovery 2D steady-state free precession imaging. Magn Reson Med 2012;68:1579–1585.
35. Deichmann R, Haase A. Quantification of T_1 values by SNAPSHOT-FLASH NMR imaging. J Magn Reson 1992;96:608–612.
36. Schmitt P, Griswold MA, Jakob PM, Kotas M, Gulani V, Flentje M, Haase A. Inversion recovery TrueFISP: quantification of T_1, T_2, and spin density. Magn Reson Med 2004;51:661–667.
37. de Rochefort L, Nguyen T, Brown R, Spincemaille P, Choi G, Weinsaft J, Prince MR, Wang Y. In vivo quantification of contrast agent concentration using the induced magnetic field for time-resolved arterial input function measurement with MRI. Med Phys 2008;35: 5328–5339.